Native amine dehydrogenases can catalyze the direct reduction of carbonyl compounds to alcohols in the absence of ammonia

Aurélie Fossey-Jouenne[1], Laurine Ducrot[1], Ewald P. J. Jongkind[2],
Eddy Elisée[1], Anne Zaparucha[1], Gideon Grogan[3], Caroline E. Paul[2]
and Carine Vergne-Vaxelaire[1]*

[1]Génomique Métabolique, Genoscope, Institut François Jacob, CEA, CNRS, Univ Evry, Université Paris-
Saclay, Evry, France, [2]Biocatalysis, Department of Biotechnology, Delft University, Delft, Netherlands, [3]York
Structural Laboratory, Department of Chemistry, University of York, York, United Kingdom

Native amine dehydrogenases (nat-AmDHs) catalyze the (S)-stereoselective
reductive amination of various ketones and aldehydes in the presence of high
concentrations of ammonia. Based on the structure of *Cfus*AmDH from
Cystobacter fuscus complexed with Nicotinamide adenine dinucleotide
phosphate (NADP$^+$) and cyclohexylamine, we previously hypothesized a
mechanism involving the attack at the electrophilic carbon of the carbonyl by
ammonia followed by delivery of the hydride from the reduced nicotinamide
cofactor on the *re*-face of the prochiral ketone. The direct reduction of carbonyl
substrates into the corresponding alcohols requires a similar active site
architecture and was previously reported as a minor side reaction of some native amine
dehydrogenases and variants. Here we describe the ketoreductase (KRED)
activity of a set of native amine dehydrogenases and variants, which proved to be significant
in the absence of ammonia in the reaction medium but negligible in its presence.
Conducting this study on a large set of substrates revealed the heterogeneity of this
secondary ketoreductase activity, which was dependent upon the enzyme/substrate
pairs considered. *In silico* docking experiments permitted the identification of some
relationships between ketoreductase activity and the structural features of the
enzymes. Kinetic studies of *Msme*AmDH highlighted the superior performance of
this native amine dehydrogenases as a ketoreductase but also its very low activity
towards the reverse reaction of alcohol oxidation.

KEYWORDS

amine dehydrogenases, ketoreduction, reductive amination, alcohol, docking

1 Introduction

To address some of the sustainable development Goals to be achived by 2030 according to
the United Nation, biocatalysis, *i.e.*, the use of enzymes for synthetic purposes, appeared as a
valid contributor for seven of them (Prather, 2020). Many of the benefits offer by biocatalysis
over conventional chemistry have been reviewed (Hollmann et al., 2020; Wu et al., 2020; Simić
et al., 2022). Among the biocatalysts studied closely, NAD(P)H-dependent oxidoreductases
performing reductive amination are established enzymes for the biocatalytic formation of
amines. Facing the importance of sustainable access to amino compounds such as bulk
chemicals and high value-added products, both the discovery of efficient enzymes and the
deep understanding of their potential, have been studied by several research teams (Ducrot

et al., 2020). Besides requiring simple starting materials (carbonyl compound, amine source), these enzymes have the major advantage of depending on an easily recyclable nicotinamide cofactor (NAD(P)H). Currently, these enzymes include amine dehydrogenases (AmDHs) from engineered L-amino acid dehydrogenases (AADHs) including an ε-deaminating L-lysine dehydrogenase (LysEDH), native amine dehydrogenases (nat-AmDHs) identified among biodiversity by (meta)genome-mining approaches and some variants, imine reductases (IREDs) and reductive aminases (RedAms) (Abrahamson et al., 2012; Abrahamson et al., 2013; Ye et al., 2015; Mayol et al., 2016; Wetzl et al., 2016; Aleku et al., 2017; Knaus et al., 2017; Roiban et al., 2017; Chen et al., 2018; Sharma et al., 2018; Chen et al., 2019; Mayol et al., 2019; Tseliou et al., 2019; Cai et al., 2020; Caparco et al., 2020; Franklin et al., 2020; Liu et al., 2020; Marshall et al., 2020; Montgomery et al., 2020; Ducrot et al., 2021; Ma et al., 2021; Yang et al., 2021; Bennett et al., 2022; Ducrot et al., 2022; Lu et al., 2022; Zhang et al., 2022). Mechanistically, the C4 atom of NAD(P)H that donates a hydride is in close proximity to the electrophilic carbon of the iminium intermediate that is formed from both substrates. Thanks to crystal structures, residues have been identified that interact with the carbonyl and/or with the amine function of the substrate/product, thus ensuring effective binding and catalysis. Therefore, theoretically, in the absence of an amine source, a similar binding of the carbonyl substrate might lead to its direct reduction into an alcohol as catalyzed by ketoreductases (KREDs). This ketone reduction is already known to be catalyzed by widely used alcohol dehydrogenases (ADHs) or KREDs, which harbor the same core Rossmann-type fold shared by the whole NAD(P)-binding domain superfamily (InterPro entry IPR036291) (An et al., 2019; de Gonzalo and Paul, 2021).

The dual reductive amination and direct ketoreduction activities of carbonyl compounds has been reported for few NAD(P)H-dependent oxidoreductases. Recently, Tseliou et al. (2020) enhanced the direct ketoreduction of aromatic aldehydes observed with LysEDH from Geobacillus stearothermophilus, through targeted protein engineering. They extensively studied the dual KRED and AmDH activity of these engineered LysEDHs and identified a dependence of this dual activity on the substrate structure with variability according to the variants. Notably, high alcohol yields were obtained for reduction of benzaldehyde and derivatives and 3-phenylpropanal, even in the presence of ammonium buffers. The wild-type LysEDH and variants LE-AmDH-v24 and LE-AmDH-v27, harboring an F173S mutation, produced the highest alcohol yields, both in ammonium and ammonium-free buffers. Interestingly, some good substrates for the AmDH reaction were poor substrates for ketoreduction in ammonia-free solution, highlighting the crucial positioning of the substrate in the active site with respect to the C4 atom of the NADH (Tseliou et al., 2020). Interestingly, no KRED activity has been described thus far with other AmDHs engineered from AADHs. However, secondary carbonyl reductase activities were reported with enzymes known to reduce C = N bonds, namely IREDs, and RedAms, but only with highly activated fluorinated acetophenones (Lenz et al., 2017; González-Martínez et al., 2020). This specific behavior, surely dependent on the higher redox potential of the carbonyl carbon, appears to be assisted by a shift of the substrate positioning resulting from an interaction of fluorine atoms with hydroxy groups of the ribose of the NADPH, thus generating the required distance from the C4 atom of NADPH to the carbonyl carbon, and so a possible direct reduction (Lenz et al., 2018;

Tseliou et al., 2020). The dual AmDH/IRED-KRED activity of such enzymes seems to be restricted to very particular cases. By contrast, secondary C = N bond reductive activity has been reported for some enzymes of the short-chain dehydrogenases/reductases enzyme superfamily (SDR), or has been introduced through protein engineering (Roth et al., 2017; Roth et al., 2020). For enzymes active towards acyclic imines, and even more towards carbonyl compounds undergoing both catalyzed imine formation and reduction, this particular feature of dual AmDH-KRED activity is thus far limited and has not been studied for a wider set of enzymes.

We have recently reported the discovery of nat-AmDHs among biodiversity and detected KRED secondary activity for several of them (Mayol et al., 2019; Caparco et al., 2020; Jongkind et al., 2022; Ducrot et al., 2022). Biocatalytic amination with MATOUAmDH2 gave rise to small amounts of alcohols (<2% of cyclohexanol at pH 8 at 1 M ammonium formate buffer) and, with the variant IGCAmDH1-W144A, 4% of octan-1-ol from octanal were detected (Ducrot et al., 2022). These results encouraged us to study this feature more specifically. Indeed, on the one hand, it is important to know whether the alcohol products can be formed in the reductive amination reactions of different types of substrates and with different nat-AmDHs, as this potentially might complicate the synthesis. On the other hand, the use of these enzymes as KREDs, or in redox-neutral cascades if a dual-active enzyme is available, can be interesting applications (Tseliou et al., 2020). Here we report the results and analysis of the KRED and AmDH activities of many nat-AmDHs and some of their already described variants. Using 19 enzymes, we have studied the correlations between their structural features and promiscuous KRED activity, while also providing some complementary kinetic studies.

2 Materials and methods

2.1 Chemicals and materials

All chemicals were obtained from commercial suppliers Sigma-Aldrich, Acros Organics, Supelco, Thermo Scientific and Combi-Blocks with the highest purity available. Glucose dehydrogenase GDH-105 was generously donated by Codexis®. GC-FID analysis were performed either on a Shimadzu GC-2010 gas chromatographs (Shimadzu, Japan) with an AOC-20i Auto injector equipped with a flame ionization detector (FID) and using nitrogen as the carrier gas (GC-FID 1), either on a Gas Chromatograph Trace 1,300 (Thermo Scientific) equipped with an autosampler injector AI/AS1310, a Flame Ionization Detector (FID) and a H_2 Generator Alliance (F-DGSi) (GC-FID 2). All samples were injected with GC quality solvents. The AmDHs used in this study have already been described (Caparco et al., 2020; Ducrot et al., 2021; Jongkind et al., 2022; Bennett et al., 2022; Ducrot et al., 2022). New batches were produced, according to the protocol already described, for IGCAmDH1, IGCAmDH1-W144A, RgnaAmDH, RgnaAmDH-W155A, MATOUAmDH2, ApauAmDH, ApauAmDH-W141A, PortiAmDH, PortiAmDH-W140A, MicroAmDH, MsmeAmDH-W141A, SgorAmDH, IGCAmDH5 and AcolAmDH (Supplementary Figure S1). For CfusAmDH, CfusAmDH-W145A, ChatAmDH, MATOUAmDH2-C148A and MsmeAmDH, previous batches obtained from previous studies and stored at −80°C were used (Jongkind et al., 2022; Ducrot et al., 2022). Spectrophotometric

assays were recorded on a Safas UVMC2 (Safas, Monaco) thermostated at 30°C with a refrigerated/heating circulator Corio CD-200F (Jubalo®, Seelbach, Germany) using microcells high-precision cell quartz with 10-mm light path (Hellma Analytics, Müllheim, Germany).

2.2 GC-FID conditions

On GC-FID 1, the samples were injected on a CP-Sil 5 CB (25 m × .25 mm × 1.20 µm) with the following parameters: Injection at 340°C, split ratio 100, linear velocity 30 cm/s, column flow 4 mL min^{-1}, nitrogen as carrier gas. Details on the oven temperature program and retention times are given in Supplementary Table S1. For chiral GC-FID analyses, the samples were injected on CP-Chirasil Dex CB (Agilent J&W) (25 m × .32 mm × .25 µm, injection at 250°C, split ratio 25, linear velocity 30 cm/s, column flow 1.68 mL/min, helium as carrier gas) for compounds **9a**, **9c**, **16a**, and **16c** and on Hydrodex β-TBDM (50 m × .25 mm × .15 µm, injection at 250°C split ratio 25, linear velocity 38 cm/s, column flow 2.35 mL/min, helium as carrier gas) for **11a** and **11c**. Details on the oven temperature program and retention times are described in Supplementary Table S2. On GC-FID 2, samples were injected on TG-35MS AMINE column (30 m × .25 mm × 1 µm; Thermo Scientific), TG-624SILMS column (30 m × .25 mm × 1.4 µm; Thermo Scientific), ZB-XLB column (20 m × .18 mm × .18 µm; Phenomenex) or CP-Chirasil Dex-CB column (25 m × .32 mm × .25 µm; Agilent) with H$_2$ as carrier gas (30 mL min^{-1}). Details on the oven temperature programs, split ratio, detector and inlet temperature and retention times are detailed in Supplementary Table S3.

2.3 pH study of ketoreductase activity with *Msme*AmDH

The reactions were performed in 100 mM NaPi buffer at pH ranging from 6.0 to 9.0 in a final volume of 1.0 mL. A solution of 10 mM substrate **15a**, .2 mM NADP$^+$, 12 mM glucose, 3 U mL^{-1} glucose dehydrogenase (GDH-105), .1 mg mL^{-1} *Msme*AmDH, 1% v/v DMSO was stirred in a thermomixer at 400 rpm and 25°C for 4 h. Extraction was carried out with 1 mL of ethyl acetate (EtOAc), the organic layer was dried over MgSO$_4$, and analyzed on GC-FID 1. Cyclohexanol (**15c**) concentrations were deduced from a calibration curve equation using 5 mM dodecane as an internal standard and **15c** reference standards. GC-FID chromatograms of reference standards, control reaction and one example of reaction with *Msme*AmDH are provided in Supplementary Figure S2.

2.4 Conversion assay for reductive amination and ketoreductase activities (GC-FID monitoring)

All the selected AmDHs were screened for conversion of a range of carbonyl-containing substrates to corresponding amines and alcohols as follows. To a reaction mixture (200 µL in 500 µL Eppendorf tubes) containing 10 mM carbonyl-containing substrate (for substrates **3**, **4**, **8**, **11**, **13**, and **14**, 200 mM stock solutions were prepared in DMSO rather than H$_2$O, with 5% v/v in the final reaction mixture), .2 mM
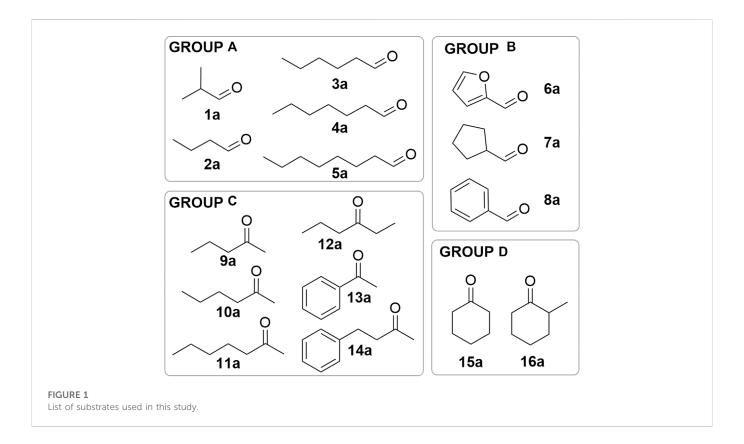
NAD$^+$, .2 mM NADP$^+$, 3 U mL^{-1} GDH-105, 12 mM D-glucose in the appropriate buffer (for reaction with ammonia/ammonium species: 2 M NH$_4$HCO$_2$/NH$_4$OH buffer at pH 8.5, for ammonia-free reactions: 100 mM sodium phosphate buffer at pH 7.5), was added .5 mg mL^{-1} of purified enzymes. For each substrate, a blank mixture was prepared in the same manner but lacking the enzyme replaced by an appropriate volume of desalting buffer used for protein purification. The reaction mixtures and the calibration points were stirred at 25°C for 24 h at 400 rpm. To 80 µL of mix reaction were added 20 µL of 10 M NaOH and an extraction with 200 µL was performed with solvent (EtOAc or methyl tert-butyl ether (MTBE)) containing known amount of internal standard (1.5 mM dodecane or toluene) related in Supplementary Table S3. The organic layers were then analyzed on GC-FID 2 according to conditions detailed in Supplementary Table S3. Product **b** and **c** concentrations were deduced from calibration curves equation prepared with various ratio of ketone/alcohol/amine (or ketone/alcohol in the case of ammonia-free reactions) in the corresponding buffer and in presence of an appropriate volume of desalting buffer. Examples of GC-FID chromatograms are provided in Supplementary Figure S3. In addition, the organic layers were analyzed on GC-FID 1 according to conditions detailed in Supplementary Table S2 with chiral columns to determine the enantiomeric and diasteroisomeric excesses of chiral alcohols. Chiral GC-FID chromatograms are provided in Supplementary Figure S4.

2.5 Determination of enantiomeric excess of alcohols

Kinetic parameters were determined by spectrophotometric NADPH-monitoring in the forward ketoreduction direction at 340 nm. The reactions were performed in 100 mM potassium phosphate buffer pH 7.5 in a final volume of 100 µL at 30°C in a spectrophotometer cell with optical paths of 1 cm. Initial rates of the reaction were measured after addition of the purified enzyme (.1 mg mL^{-1}) with various concentrations of **15a** (or NADPH) and saturated concentrations of NADPH at .2 mM (or **15a** at 2 mM). The uncertainties are those generated by the fitting and the data are averages of three independent experiments. The conditions, fitting and determination of kinetic parameters were performed with Sigma Plot software and plots are provided in Supplementary Figure S5.

2.6 Specific activities in ketoreduction and alcohol oxidation catalysis

The reactions were conducted in duplicate at 30°C in a thermostated spectrophotometric cell (10 mm light path) in a final reaction volume of 100 µL. For the KRED activity, the reactions were performed in potassium phosphate buffer pH 7.5 with .2 mM of NADPH and .1–.3 mg mL^{-1} of enzyme (*Msme*AmDH, MATOUAmDH2, *Cfus*AmDH, IGCAmDH1, *Micro*AmDH). Initial rates of the reaction were measured at 340 nm after addition of 2–10 mM of substrate (**6a**, **7a**, and **15a**) to determine the specific activity of the enzyme according to Beer—Lambert's law and the molar absorptivity of β-NADPH (ε = 6,220 M^{-1} cm^{-1}) after subtraction of the slope obtained under the same conditions except without enzyme. The calculated specific activities are detailed in

FIGURE 1
List of substrates used in this study.

Supplementary Table S4. For alcohol oxidation activity, the reaction were performed in 100 mM Tris-HCl pH 8.6 buffer with .2 mM of NADP⁺ and 2 mM of **7c** or **15c**. Initial rates of the reactions were measured at 340 nm after addition of 1 mg mL⁻¹ of *Msme*AmDH to determine the specific activity as mentioned above after subtraction of the slope obtained under the same conditions but lacking substrate.

2.7 Docking experiments

For study cases in ammoni-free buffer, the products **6a**, **6c**, **7a**, **7c**, and **15c** were docked into the closed conformations of structures of MATOUAmDH2-NADP (PDB ID: 7ZBO), *Msme*AmDH-NADP (PDB ID: 6IAQ) and *Cfus*AmDH-NADP-**15b** (PDB ID: 6IAU) after removal of the amine **15b**, and on models of *Rgna*AmDH-NAD, *Micro*AmDH-NAD(P) and IGCAmDH1-NAD (Mayol et al., 2019; Caparco et al., 2020), minimized beforehand to obtain the more favored positioning of the nicotinamide cofactor from its copied position in the *Cfus*AmDH-NADP structure. The latter were previously minimized without restraints, using the YASARA2 force field within YASARA, after addition of the nicotinamide cofactor copied from the *Cfus*AmDH-NADP structure (Krieger et al., 2009). For study cases in presence of ammonia/ammonium with *Rgna*AmDH, the model of *Cfus*AmDH-**15a**-NH₄, already published, was used as a template to paste the ammonium molecule, after alignment of models using PyMOL Molecular Graphics System (Version 2.0 Schrödinger, LLC) (Mayol et al., 2019). NAD cofactor was built from the *Cfus*AmDH-NADP structure by replacing the phosphate group (P2B, O1X, O2X and O3X atoms) with a hydrogen atom. The ligand PDB files were generated using the CORINA Molecular Online Tool (https://

demos.mn-am.com/corina.html). With AutoDockTool, the docking simulations were performed on rigid structures, with no flexibility given to any catalytic pocket residues (Morris et al., 2009). The box was centered in the active site with the following size: 34, 36, 30 (36, 38, 30 in the case of dockings in presence of NH₃) (Autodock parameters). The number of Genetic Algorithm (GA) runs was fixed at 10 using the Lamarckian GA (4.2). The 10 ligand conformations obtained were then analyzed on PyMOL Molecular Graphics System (Version 2.0 Schrödinger, LLC).

3 Results and discussion

3.1 Conversion data in alcohols and amines

We conducted this study with 12 characterized nat-AmDHs, i.e. *Chat*AmDH, IGCAmDH1, *Rgna*AmDH, MATOUAmDH2, *Cfus*AmDH, *Apau*AmDH, *Porti*AmDH, *Micro*AmDH, *Msme*AmDH, *Sgor*AmDH, IGCAmDH5 and *Acol*AmDH, in addition to the recently described seven variants corresponding to *Cfus*AmDH-W145A (Ducrot et al., 2022). We tested these 19 enzymes toward a large panel of carbonyl substrates at 10 mM concentration (Figure 1). Group A comprises alkyl linear aldehydes (isobutyraldehyde (**1a**), butanal (**2a**), hexanal (**3a**), heptanal (**4a**) and octanal (**5a**)), group B substituted aldehydes (furfural (**6a**), cyclopentanecarbaldehyde (**7a**) and benzaldehyde (**8a**)), group C linear ketones (pentan-2-one (**9a**), hexan-2-one (**10a**), heptan-2-one (**11a**), hexan-3-one (**12a**), acetophenone (**13a**) and 4-phenylbutan-2-one (**14a**)) and group D cyclic ketones (cyclohexanone (**15a**) and 2-methylcyclohexanone (**16a**)). The alcohol **1c–16c** and/or amine **1b–16b** products were semi-
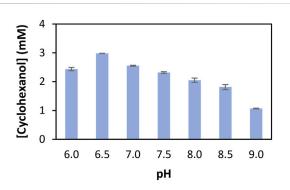
FIGURE 2
pH effect on conversion of cyclohexanone (15a) into cyclohexanol (15c) in ammonia-free buffer. Conditions: 100 mM NaPi buffer, pH 6.0–9.0, 12 mM glucose, 6 U mL^{-1} GDH-105, .2 mM NADP$^+$, .1 mg mL^{-1} *Msme*AmDH, 10 mM cyclohexanone 15a, 1% v/v DMSO, 25°C, 400 rpm, 4 h. Cyclohexanol is quantified with calibration curves by GC-FID (GC-FID 1). Error bars represent standard deviations of two independent experiments.

quantified in two reaction conditions (condition a: Buffer with ammonia/ammonium species; conditions b: Buffer without ammonia) by GC-FID monitoring, with a mix of NAD$^+$ and NADP$^+$ cofactors, internally recycled with glucose dehydrogenase GDH-105. The specific activities of some of the enzyme/substrate pairs were also determined (Supplementary Table S4).

For ammonia-free reactions, previous data reported by (Tseliou et al., 2020) demonstrated higher apparent rates of reduction at pH 7.0 compared to higher pH, and no preferred type of buffer in cofactor-recycling conversion studies. With the objective of achieving the best conversions into alcohols in condition b, we studied the effect of pH on the alcohol formation with the couple 15a/*Msme*AmDH in sodium phosphate buffer. The reaction conditions (quantity of enzymes and duration) were deliberately adapted to deviate from quantitative conversions and thus to better visualize the differences according to the pH. As depicted in Figure 2, the alcohol amount 15c was quite similar in the pH range 6.0–7.5 and decreased progressively above pH 8.0. The screening for KRED activity was also done at pH 7.5 unlike the one for AmDH activity performed at pH 8.5 as already published (Mayol et al., 2019).

All the conversions deduced from calibration curves of standard alcohols and amines are presented in Figure 3. Despite alcohols peaks observed in blank reactions lacking enzymes, especially with aldehydes, the alcohol formations are enzymatic and present after subtraction of these blank controls (Supplementary Figure S3). Importantly, in 2 M ammonium buffer (conditions a), the AmDH activity strongly outperformed the KRED one, as, in most cases, no or only traces of alcohol could be detected (<1% conversion). The saturated ammonia/ammonium concentration promotes the amination reaction, presumably minimizing the "free" carbonyl substrate in the active site and so its direct reduction (Mayol et al., 2019). This KRED activity, specific to ammonia-free buffer, differs from the KRED side activity of wild-type or some engineered LysEDHs observed in ammonium buffer for some substrates. For example, 8a was converted into 17% of 8b and 23% of 8c in 2 M ammonium formate buffer with wild-type LysEDH (Tseliou et al., 2020). Here, none of the tested enzymes was revealed to display higher promiscuous KRED activity than AmDH one in ammonium buffer,

except *Porti*AmDH, which displayed 3.4% conversion of 5a into 5c but no conversion into 5b. More notable KRED activities (conversions of 3.1%–9.3%) were reached with variants, even if they were still lower than the AmDH ones.

On the contrary, in ammonia-free buffer (condition b), alcohols were detected, even up to significant amounts. It appeared that, in general, the amounts of alcohol formed were very variable. This was not only linked to the identity of the enzyme itself, but also to the enzyme/substrate couple. Among all the tested substrates, each enzyme displayed notable KRED activity (>.5 mM of alcohol formed) with at least one substrate. Higher alcohol formation and a higher number of accepted substrates were obtained with some enzymes compared with others. *Rgna*AmDH, MATOUAmDH2, *Porti*AmDH, *Micro*AmDH and *Msme*AmDH display high promiscous KRED activity in ammonium-free buffer, with up to 96% of alcohols formed. Generally, for wild-type enzymes, we observed much higher AmDH activity in ammonia-rich buffer than ketoreduction in ammonia-free buffer, but with variabilities depending on the type of substrate. For the short substrates 1a and 2a of group A, the conversions into alcohols in condition b were at least twice lower than the conversions into amines in condition a. Up to around conversions of 40% were nevertheless obtained, for example for 1a into 1c with *Msme*AmDH, *Rgna*AmDH and *Cfus*AmDH. For enzymes active toward longer aldehydes, the AmDH activity was 6–20 times higher than the KRED one; no more than 10% of alcohol 3c were obtained in condition b. For group B, unsaturated aldehydes 6a and 8a were not reduced, or only in very low amounts, despite many of the tested enzymes displayed high conversions to the corresponding amines 6b and 8b in ammonia-rich buffer. Specific activities towards 6a were all below .6 mU mg^{-1}, thus in accordance with conversion results (Supplementary Table S4). The KRED activity was observed only for cyclopentanecarbaldehyde 7a, with differing AmDH/KRED activity ratios dependent on the enzymes. *Rgna*AmDH and MATOUAmDH2 appeared as the enzymes with the higher KRED promiscuous activity for this substrate with 16%–32% and 23%–27% conversions of 7a into 7c respectively, and IGCAmDH1 and *Chat*AmDH the less active ones for the direct reduction while forming 63%–76% of cyclopentanecarbamine (7b). The specific activities determined with 7a in ammonia-free buffer correlates with such KRED activity data, with .4 and 14.6/58.4 mU mg^{-1} measured for IGCAmDH1 and *Rgna*AmDH/MATOUAmDH2 respectively. In group C, for 9a, the KRED activity was significant in the cases of enzymes displaying high conversions in reductive amination, with AmDH/KRED activity ratios of around 4/1 for *Cfus*AmDH and *Micro*AmDH to 2/1–1/1 for *Porti*AmDH and *Msme*AmDH respectively. For example, 53% conversion into 9b vs. 54% into 9c, in the respective ammonia-rich and ammonia-free conditions, were obtained with the couple 9a/*Porti*AmDH. This trend was not shared for hexan-3-one (12a), for which no alcohol 12c was detected despite high amine 12b formation for *Porti*AmDH, *Micro*AmDH, and *Msme*AmDH. For the other substrates of this group displaying activities only with variants, the amounts of alcohol were only significant with *Cfus*AmDH-W145A, with 17%–36% of 11c and 14c, when 54% and 53%–70% of corresponding amines 11b and 14b were formed. For *Apau*AmDH-W141A and *Micro*AmDH-W141A, no or only low amounts of these alcohols were detected, while the AmDH activities induced conversions above 20%. For cyclic ketones of group D, all

Group	product	Chat AmDH WT	IGC-AmDH1 WT	IGC-AmDH1 W144A	Rgna AmDH WT	Rgna AmDH W155A	MATOUAmDH2 WT	MATOUAmDH2 C148A	Cfus AmDH WT	Cfus AmDH W145A	Apau AmDH WT	Apau AmDH W141A	Porti AmDH WT	Micro AmDH WT	Micro AmDH W141A	Msme AmDH WT	Msme AmDH W141A	Sgor AmDH WT	IGCAmDH5 WT	Acol AmDH WT
A	1b[a]	62.5	51.7		65.9		61.4		63.1		60.0		44.7	34.7		58.6		41.0	54.3	57.6
	1c[a]	nd	nd		nd		nd		nd		nd		nd	nd		nd		nd	nd	nd
	1c[b]	12.1;11.4	12.2;8.7		39.8;29.0		35.4;27.9		38.8;23.4		27.7;26.3		24.7;20.0	21.3;18.6		40.9;26.1		18.2;12.6	27.5;11.1	25.3;10.5
	2b[a]	45.7	53.5		54.7		51.9		49.0		40.3		35.8	33.1		46.9		38.0	44.3	39.0
	2c[a]	nd	nd		nd		nd		nd		nd		nd	nd		nd		nd	nd	nd
	2c[b]	7.0;5.0	10.9;2.9		29.9;24.6		32.2;25.5		27.4;15.0		13.5;9.9		22.7;19.5	18.8;14.3		30.8;18.2		12.2;5.6	8.7;3.2	7.6;4.9
	3b[a]	4.6	2.4	29.7	12.5	85.6	72.7	79.2	39.9	99.5	5.3	59.6	60.8	65.1	2.0	54.9	3.0	4.2	2.0	1.2
	3c[a]	nd	nd	1.8	<1	nd	nd	nd	nd	nd	nd	nd	nd	nd	<1	nd	nd	<1	<1	<1
	3c[b]		4.8	9.0;5.0	5.5	5.2	5.2	1.3	2.8	8.8;5.0		11.6;8.8	2.9	6.0		4.0		4.8	2.5	6.9
	4b[a]	0.1	0.1	26.9	0.6	36.6	26.9	32.5	2.3	40.4	0.1	34.4	7.9	18.1	0.6	6.0	2.0			
	4c[a]	2	1.6	3.2	2.7	0.8	0.8	0.9	1.2	0.5	1.4	0.8	3.1	1.5	3.3	1.3	2.1			
	4c[b]																			
	5b[a]	nd	nd	32.3	nd	39.1	13.8	21.5	nd	38.8	nd	34.9	nd	3.1	5.2	nd	6.5			
	5c[a]	<1	<1	4.0	3.2	<1	<1	1.2	<1	nd	<1	<1	3.4	<1	2.8	<1	1.4			
	5c[b]		16.4;5.4		5.5					34.6;8.2		23.9;9.0			4.9		4.7			
B	6b[a]	76.3	62.7	<1	68.2	3.2	79.7	72.4	83.5	13.3	77.3	1.5	44.5	37.2	<1	78.9	<1	27.0	28.9	16.9
	6c[a]	nd	nd	nd	nd	nd	nd	nd	nd	nd	nd	nd	nd	nd	nd	nd	nd	nd	nd	nd
	6c[b]	nd	nd	nd	nd	nd	nd		nd	nd	nd	nd	nd	nd	nd	nd		nd	nd	nd
	7b[a]	41.1	44.6	1.3	47.1	25.8	49.2	54.3	51.3	18.6	43.7	12.3	49.4	48.3	47.5	56.0	21.8	16.8	62.3	48.7
	7c[a]	<1	<1	1.0	nd	5.8	nd	nd	nd	1.7	nd	6.6	nd	<1	nd	<1	9.3	nd	nd	nd
	7c[b]	4.8	4.4	6.6	31.7;15.7	4.1	27.1;23.2		11.7;10.6	4.1	7.6;6.2	6.1	29.7;13.2	29.4;15.4	5.3	19.6;16.0	4.5	4.0	3.3	4.3
	8b[a]	9.7	14.7	3.7	76.5	2.6	56.9	55.3	79.0	14.8	22.2	1.7	23.5	14.5	nd	37.2	nd	30.9	12.7	nd
	8c[a]	1.2	<1	2.9	<1	3.3	<1	<1	<1	<1	<1	2.7	<1	1.1	nd	<1	nd	nd	nd	nd
	8c[b]	nd	nd	nd	nd	nd	nd		nd	nd	nd	nd	nd	nd	nd	nd		nd	nd	nd
C	9b[a]	nd	nd		9.2		20.6		43.0		<1		53.5	50.8		43.8				
	9c[a]	nd	nd		nd		nd		nd		nd		1.4	nd		<1				
	9c[b]	nd	nd		<1		1.6		9.6;9.5 (>99)		nd		54.2;39.2 (>99)	11.5;11.4 (>99)		31.6;22.6 (>99)				
	10b[a]	nd	nd	nd	<1		<1		2.0 (77.5)	3.0 (91.8)	3.1(94.7)	39.7 (99.3)	nd	4.0 (99.2)	26.5 (79.4)	22.6 (94.6)	1.2 (>99.9)	8.4 (98.8)	<1	nd	nd	nd
	10c[a]	nd	nd	nd	nd	nd	nd	nd	nd	nd	nd	nd	nd	nd	nd	nd	nd	nd	nd	nd
	10c[b]									2.9			6.9		<1		2.3		nd	nd	nd
	11b[a]	<1	<1	<1	<1	<1	<1	<1	<1	53.7 (99.7)	<1	18.5 (99.3)	4.2 (33.0)	1.5	<1	<1	4.6 (>99.9)			
	11c[a]	nd	nd	nd	nd	nd	nd	nd	nd	<1	nd	nd	<1	nd	nd	nd	nd			
	11c[b]			nd		nd			33.2;16.9 (>99)		<1			nd		<1				
	12b[a]	nd	nd	nd	nd	<1	12.4 (38.2)	9.0 (12.1)	5.8 (29.1)	1.7 (91.3)	<1	nd	46.5 (13.9)	51.2 (87.6)	4.4 (>99.9)	39.1 (88.4)	<1	nd	nd	nd
	12c[a]	nd	nd	nd	nd	nd	nd	nd	nd	nd	nd	nd	1.2	nd	nd	nd	nd	nd	nd	nd
	12c[b]						nd		nd		nd		nd	nd		nd		nd	nd	nd
	13b[a]						<1	<1	<1	2.2 (96.9)	<1	<1	7.4 (97.0)	13.9 (99.1)	<1	1.9 (96.5)	<1	nd	nd	nd
	13c[a]						nd	nd	nd	nd	nd	nd	nd	nd	nd	nd	nd	nd	nd	nd
	13c[b]													<1				nd	nd	nd
	14b[a]						<1	<1	<1	69.5;52.5 (99.6)	<1	31.2;22.2 (99.2)	2.4 (49.6R)	42.1;28.1 (95.5)	<1	46.4;34.1 (99.9)	<1			
	14c[a]									nd		nd				nd		nd		
	14c[b]									35.8;24.1 (99.5)		nd				nd		6.0		
D	15b[a]	19.3	19.5		89.2		87.4		86.7		44.7		86.0	88.5		87.8		25.8	33.5	9.2
	15c[a]	nd	nd		nd		nd		nd		nd		nd	nd		nd		nd	nd	nd
	15c[b]	<1	nd		17.2;15.5		30.5;27.5		>99;80.5		11.4;11.1		>99;77.9	>99;78.9		>99;78.7		1.7	2.8	<1
	16b[a]	<1	<1		5.7		52.9		55.9		5.4		62.5	62.6		61.7		<1	<1	nd
	16c[a]	nd	nd		nd		<1		<1		nd		nd	nd		nd		nd	nd	nd
	16c[b]	nd	nd		<1		24.8;40.0 (78(83):22(92))		15.0;28.0 (60(81):40(80))		nd		70.0;96.0 (75(73):25(81))	69.3;87.0 (80(74):20(97))		75.3;90.0 (82(83):18(80))		nd	nd	nd

FIGURE 3

Conversion of carbonyl substrates 1a−16a into amines 1b−16b and alcohols 1c−16c in ammonium buffer, and in alcohols 1c−16c in ammonium buffer and ammonia-free buffer, with described AmDHs. Conditions: 10 mM carbonyl substrate, .5 mg mL^{-1} AmDH, .2 mM NAD$^+$, .2 mM NADP$^+$, 3 U mL^{-1} GDH-105, 12 mM glucose in 2 M ammonium formate buffer pH 8.5 (condition a) or in 100 mM sodium phosphate buffer pH 7.5 (condition b). Reactions were performed in 100 µL final volume in 500 µL Eppendorf tubes for 24 h at 25°C at 400 rpm and analyzed by GC-FID (GC-FID 2). Yields (%) provided were deduced from calibration curves with reference standards. Duplicated experiments in condition b were performed when conversions into alcohols 1b−16c were >7% in the first screening. Both values are indicated. Color code from dark green (high conversions) to light green (low conversions) helps for reading. a = conditions a; b = conditions b. nd = not detected (<.1% i.e., .01 mM). Empty boxes = not tested. Enantiomeric excesses (ee) of alcohols are provided between brackets in case of prochiral substrates, for conversions >10% (after analyses by GC-FID (GC-FID 1)). For 16c, cis (ee$_{(S,R)}$): trans (ee$_{(S,S)}$) ratios are indicated.

the highyl active AmDHs displayed high promiscuous KRED activity, giving particularly nearly total conversion in cyclohexanol 15c with CfusAmDH, MicroAmDH, MsmeAmDH and PortiAmDH in ammonia-free buffer. These results were in line with the high KRED specific activities of 39.4, 510.6 and 235.2 mU mg^{-1} measured in ammonia-free buffer with 15a for the first three, respectively (Supplementary Table S4).

3.2 Stereochemistry

In the case of prochiral substrates (group C and D except 15a), the enantiomeric excesses (ee) were measured when >1 mM of alcohols (>10% conversion) were formed. As for the AmDH activity, the (S)-configuration was obtained with ee of (S)-alcohols 9c and 11c >99%. We can conclude a high (S)-selectivity for the promiscuous KRED

TABLE 1 Kinetic parameters of *Msme*AmDH for the KRED activity.

	k_{cat} (s^{-1})	K_m (mM)	k_{cat}/K_m (s^{-1} M^{-1})
cyclohexanone 15a	.17	.25	667
NADPH	.14	.04	4,155

Kinetic parameters were measured in a 100 μL final volume in 100 mM potassium phosphate buffer at pH 7.5 at concentrations of .05–2 mM of 15a and .005–.3 mM of NADPH.

activity of these AmDHs. In the case of the chiral substrate **16a**, the *cis*-configuration was the major but not exclusive form (*cis:trans* ratio from 60:40 to 82:18) of the alcohol product **16c**, with a moderate to high preference for the (*S*)-configuration at the quaternary carbon created (*ee* (*S,R*) = 73–83%; *ee* (*S,S*) = 80–97%)) (Figure 3; Supplementary Figure S6).

3.3 Kinetic parameters of *Msme*AmDH for its promiscuous KRED activity

The Michaelis-Menten parameters were determined for *Msme*AmDH for the reduction of cyclohexanone **15a** to cyclohexanol **15c** to provide a comparison to the values previously reported for its reductive amination into **15b** (Table 1; Supplementary Figure S5) (Mayol et al., 2019). Indeed, *Msme*AmDH was able to catalyze the conversion of this substrate for both reactions in high yields. In the absence of ammonia and at pH 7.5, the K_m for cyclohexanone **15a** was slightly lower than in amination condition (.25 mM and .55 mM respectively). A similar observation was made for the K_m of the cofactor NADPH (.04 and .06, respectively). The k_{cat} being seven times lower, the resulting catalytic efficiency was approximately two times lower for **15a** for the KRED activity over the AmDH one, and nearly identical for NADPH. *Msme*AmDH displayed very slow catalysis of oxidation with a specific activity for **15c** reaching only .4 mU mg^{-1}, preventing any accurate determination of kinetic parameters. No oxidation activity could even be detected for **7c**, whose corresponding ketone **7a** nevertheless emerged as a very good substrate in reduction condition.

3.4 *In silico* analysis

In an attempt to link the *in vitro* data to the active-site characteristics of the enzymes, some structural analysis and docking experiments were performed on the closed conformations of structures of MATOUAmDH2-NADP, *Msme*AmDH-NADP and *Cfus*AmDH-NADP, and on minimized models of *Rgna*AmDH-NAD, *Micro*AmDH-NAD(P), IGCAmDH1-NAD and *Rgna*AmDH-NAD-NH$_4^+$ for studies in presence of ammonia/ammonium species (see *Material and methods*). We confirmed the minimization step by comparing the conformations before and after minimization for the X-raystructure of *Cfus*AmDH with NADP$^+$. The greatest difference was seen for the ribose of NADP$^+$ with a shift of 1.2 Å, but more importantly, no shift in orientation of all the residues involved in the pocket and the nicotinamide part were observed (Supplementary Figure S6). In addition, the minimized model of MATOUAmDH2 was compared to its X-raystructure (PDB ID: 7ZBO) recently published (Bennett et al., 2022). Some important shifts were observed in the more flexible part such as Y176, residue

too far from the reacting part to be discussed in this paper. For the residues surrounding the substrate/product, no drastic shifts were generated, but the notable depicted ones (.7–1.5 Å) have to be considered for discussion results (Supplementary Figure S7). The following molecules were docked: **6a–c**, **7a–c**, and **15a–c**; and the top ten conformations were considered (Table 2; Supplementary Figure S8). We noticed that the docked aldehydes or ketones **a** should be analyzed more carefully, as the obtained conformations were often not in agreement with the conformations of the corresponding products and mechanism. For example, the docked conformations of **15a** displayed the carbonyl function "in the lower front" of the pocket, certainly due to interactions with the NH backbone of Q137 (*Msme*AmDH numbering) and amide of the cofactor. In these conformations, the distances between the reactive carbon and the C4 of the nicotinamide are in the 4.6–5.1 Å range, therefore in disagreement with observed reduction (Supplementary Figure S9). We can notice that in the case of MATOUAmDH2, the docked **7a** and **15a** were flipped, with the carbonyl oriented to the "right" of the pocket, *i.e.*, to His184 and Tyr171. The higher space available in this bigger pocket enables such orientation, in a conformation more similar to the one of the alcohol product, which may induce higher efficiency of MATOUAmDH2 for the reduction compared to other enzymes such as *Msme*AmDH (Supplementary Figure S10) (Bennett et al., 2022). Precisely for cyclopentanecarbaldehyde **7a**, KRED specific activities were ten-fold higher for MATOUAmDH2 compared to *Msme*AmDH (58.4 vs. 5.2 mU mg^{-1}) (Supplementary Table S4).

First, looking at the distance between the carbon bearing either the alcohol or the amine and the C4 atom of the nicotinamide (hydride donor), we noticed that they are quite similar for a couple alcohol/amine and in an appropriate range for hydride delivery in many cases (3.3–4.2 Å) (Agarwal et al., 2000). The main interaction promoting lower energy conformations is indeed the hydrogen bond between labile hydrogen of alcohol or amine with the oxygen atom of the catalytic residue Glu104 (*Msme*AmDH numbering), which "sticks" the carbon atom carrying this function at a very similar position, and therefore at a similar distance with the NADPH C4 atom hydride. Despite being in the same range, notable trends can be established from small differences for this key distance, all the more so if we coupled the criterion of calculated energies of the top conformations (Table 2; Supplementary Figure S8). Globally, the alcohol conformations were of higher energies than the amine ones, and the gain of energies between carbonyl substrates and alcohol vs. amine were lower (.05 to −.22 vs. −2.05 to −2.29 kJ mol^{-1}), which could be in agreement with the higher amount of amine formed compared to alcohol. In the case of **7c**, lower average distances of 3.90 and 3.91 Å were measured for the favored "up" conformations for *Msme*AmDH and *Rgna*AmDH respectively, enzymes with high promiscuous KRED activities, whereas slightly higher distances (3.8–4.6 Å, average value = 4.11 Å) were measured for IGCAmDH1 displaying very low

TABLE 2 C4N-C(OH) distances and related energies of the corresponding top 10 docked conformations of alcohols 6c, 7c and 15c into some studied nat-AmDHs.

	6c	7c	15c
*Rgna*AmDH		3.91 (−5.18)	3.66 (−5.51)
MATOUAmDH2	4.27 (−3.67)	4.12 (−4.71)	3.80 (−5.00)
*Micro*AmDH		4.59 (−5.08)	3.98 (−5.42)
*Msme*AmDH	3.77 (−4.23)	3.90 (−5.40)	3.64 (−5.82)
*Cfus*AmDH	3.52 (−4.21)	3.64 (−5.24)	3.78 (−5.53)
IGCAmDH1		4.11 (−4.97)	4.14 (−5.17)

Distances are expressed in Å. Energy are expressed in kJ mol⁻¹, and indicated in brackets.
[a]Flipped conformations. Average values are provided. For detailed results for each 10 conformations and results on 6a–6b, 7a–7b, 15a–15b, see Supplementary Figure S8.
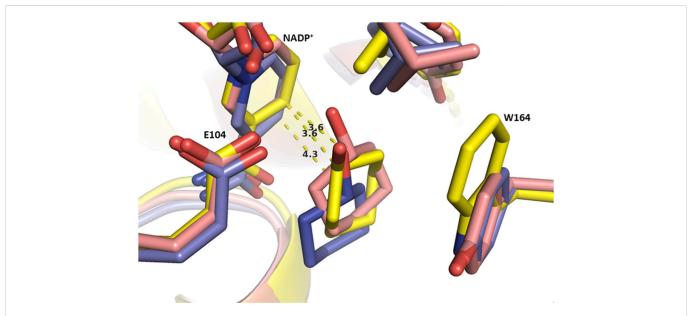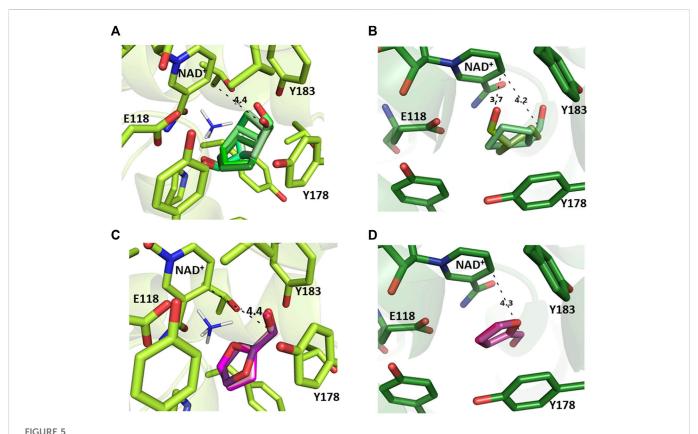

FIGURE 4
C4N-C(OH) distances for *Msme*AmDH (yellow), *Cfus*AmDH (pink) and IGCAMDH1 (purple) with selected conformations of docked cyclohexanol (15c). Distances are in Å. Surrounding residues are labelled only for *Msme*AmDH for clarity.

conversion and specific activity toward **7a** (Table 2; Supplementary Table S4). Having in mind that a distance of 4.3 Å is already too distant to postulate a direct hydride transfer, most of the conformations obtained with the latter were not in accordance with a possible reduction. Moreover, for the enzyme IGCAmDH1 with low promiscous KRED activity, energies were all higher than −4.97 kJ mol⁻¹, unlike the others which were below −5.1 kJ mol⁻¹, reaching −5.46 kJ mol⁻¹ for *Msme*AmDH with good promiscuous KRED activity. For MATOUAmDH2, and to a lesser extent *Micro*AmDH, bearing bigger catalytic pockets, these relationships were not found. Such observation could also be made for cyclohexanol (**15c**) where distances of 3.6–3.8 Å, associated with lower energies (−5.42 to −5.83 kJ mol⁻¹), were calculated for nearly all the top ten conformations for *Micro*AmDH, *Msme*AmDH, *Cfus*AmDH displaying high promiscuous KRED activities, whereas longer distances (3.9–4.6 Å) with higher energy (−5.19 to −5.15 kJ mol⁻¹) were measured for IGCAmDH1, for which only traces of **15c** and specific activitiy of .5 mU mg⁻¹ were obtained in *in vitro* experiments (Figure 4; Supplementary Figure S8.

In the case of *Rgna*AmDH, five of the ten top conformations of **15c** displayed distances of 3.4–3.5 Å whereas only 15.5%–17.2% alcohol were formed experimentally and a moderate specific activity of 2.6 mU mg⁻¹ was calculated with **15a**. The remaining other five conformations were inappropriately flipped which may reflect an inferior suitability of this active site for **15c**, as observed for *Cfus*AmDH for **7c**. Interestingly, the average energy for **7c** (−4.71, −5.41, and −5.23 kJ mol⁻¹) and **15c** (−5.00, −5.82, and −5.53 kJ mol⁻¹) were much lower than the ones for **6c** (−3.67, −4.23, and −4.21 kJ mol⁻¹) with, respectively MATOUAmDH2, *Msme*AmDH, and *Cfus*AmDH. Combined with the fact that the energy difference between ketone/aldehyde substrates and alcohol products are negative for **7** and **15** (−.07 to −.21 kJ mol⁻¹), while being positive for **6** (.05 kJ mol⁻¹) unlike the furfural **6a**/furfurylamine **6b** one (−2.05 kJ mol⁻¹), this trend can be linked to the low specific activities with **6a** compared to **7a** and **15a** and the absence of **6c** in conversion experiments, compared to notable amounts of **7c** and **15c** (conversions of 10.6%–23.2% of **7a** and 30.5—>99% of **15a** into **7c** and **15c,** respectively).

FIGURE 5
Active sites of *Rgna*AmDH docked **(A)** with NH_4^+ and 7a; **(B)** without NH_3 and 7a; **(C)** with NH_4^+ and 6a; **(D)** without NH_3 and 6a. Distances are in Å. For clarity, only one conformation is shown in the case of several almost identical conformations.

To give some insights into the differences observed in conversions into alcohol in the presence or absence of ammonia, docking experiments were performed on *Rgna*AmDH with **6a** and **7a**, with or without NH_4^+ docked inside the active site, using the model of *Cfus*AmDH-**15a**-NH_4^+, already published, as a template (Mayol et al., 2019). With docked NH_4^+, the reactive carbon of **7a** was too far from the C4 nicotinamide in all the conformations (−4.4–5.1 Å) to allow reduction, whereas these distances (3.7 Å for correct conformations) in absence of NH_3 were in accordance with experimentally observed KRED activity (conversion 32%) and specific activities (14.6 mU mg^{-1}). For **6a**, the calculated distances (4.3–4.4 Å) were in each case incompatible with KRED activity both in ammonia-free or ammonia-rich conditions, as observed in the *in vitro* experiments (Figures 3, 5; Supplementary Figure S4).

4 Discussion

Based on the determined kinetic parameters, *Msme*AmDH performs both carbonyl reduction and reductive amination in the same range, in absence or presence of ammonia source respectively. It differs from LE-AmDH-v1, which was reported to act preferentially as an AmDH with benzaldehyde, mainly due to a much higher k_{app} (Tseliou et al., 2020). However, the effect on K_m was similar as LE-AmDH-v1 also exhibited four-fold better K_{mapp} for the reduction, as for *Msme*AmDH. Compared to the well described alcohol dehydrogenase (ADH) from *Ralstonia*

sp. (RADH), which was shown to prefer aromatic and cyclic aliphatic compounds, the K_m for **15a** was 60 times lower for *Msme*AmDH than for RADH (10.8 mM for RADH at the same pH 7.5). The K_m for the NADPH cofactor was more in the same range (.008 mM for RADH). The affinity of *Msme*AmDH for cyclohexanone **15a** in the reduction condition at pH 7.5 was also higher than for other ADHs/KREDs, such as that of *Methanobacterium palustre* (K_m = 6.5 mM), despite a much lower velocity (v_{max} = 30 U mg^{-1}; k_{cat} = 86 s^{-1}) (Josef and Winter 1991). The catalysis is extremely less reversible for *Msme*AmDH than for both RADH and ADH from *Mb. Palustre,* reported to catalyze both the reduction of **15a** and the oxidation, even if the reduction was faster (2.5-fold at pH 9.0 in Tris-HCl buffer and 18-fold at pH 7.5 respectively) (Kulig et al., 2013). *Msme*AmDH, and by extension the nat-AmDHs, therefore appear as good enzymes for the reduction of ketones to alcohols with the particularity of having almost no activity in the reverse direction of oxidation. The docking experiments carried out in this study allowed to formulate hypotheses for the KRED promiscuous activity of some nat-AmDHs with a few substrates, based on distance and energie differences. But highlighting some key residues responsible for variations in AmDH/KRED activity ratios, *via* different product positioning, remains a challenge because the first layer in enzymes with either low or high promiscuous KRED activities are all very similar. Further analysis such as molecular dynamics at different pH could provide clues. The dual activity shown in this study raises the

question of whether there is a link between the two families of enzymes nat-AmDHs and KREDs. Nevertheless, the demonstrated catalytic glutamate, not present in KREDs and not required in the ketoreduction mechanism, does not point to an evolutionary relationship. This hypothesis will perhaps be clarified when the metabolic role of nat-AmDHs will be elucidated, which is not currently the case for *Cfus*AmDH and *Msme*AmDH homologs.

This study highlights a key feature of the native AmDH family, *i.e.*, the potential of some of these enzymes to perform ketoreduction, even quite efficiently for some substrate/enzyme couples. Such behavior is not detrimental for their use as biocatalysts for amine synthesis as no, or only traces, of the corresponding alcohols could be detected in the presence of excess of ammonia, required for the amination reaction. On the contrary, this dual activity can be beneficial in some synthetic schemes where the AmDH and KRED activities could be alternatively turned off or turned on depending on the reaction conditions. Nevertheless, their very low activity in the oxidative direction would prevent their use in one pot neutral hydrogen-borrowing cascades with a single enzyme, as already reported with LysEDH variants.

Data availability statement

The original contributions presented in the study are included in the article/Supplementary Material, further inquiries can be directed to the corresponding author.

Author contributions

CV-V conceived the project. AF-J, LD, and EJ designed and conducted the experiments, with input of EE, and CV-V analyzed data with input of AZ, GG, and CP. CV-V wrote the manuscript with input from all the authors. All authors read and approved the final manuscript.

Conflict of interest

The authors declare that the research was conducted in the absence of any commercial or financial relationships that could be construed as a potential conflict of interest.

Publisher's note

All claims expressed in this article are solely those of the authors and do not necessarily represent those of their affiliated organizations, or those of the publisher, the editors and the reviewers. Any product that may be evaluated in this article, or claim that may be made by its manufacturer, is not guaranteed or endorsed by the publisher.

Supplementary material

The Supplementary Material for this article can be found online at: https://www.frontiersin.org/articles/10.3389/fctls.2023.1105948/full#supplementary-material

References

Abrahamson, M. J., Vazquez-Figueroa, E., Woodall, N. B., Moore, J. C., and Bommarius, A. S. (2012). Development of an amine dehydrogenase for synthesis of chiral amines. *Angew. Chem. Int. Ed.* 51 (16), 3969–3972. doi:10.1002/anie.201107813

Abrahamson, M. J., Wong, J. W., and Bommarius, A. S. (2013). The evolution of an amine dehydrogenase biocatalyst for the asymmetric production of chiral amines. *Adv. Synth. Catal.* 355 (9), 1780–1786. doi:10.1002/adsc.201201030

Agarwal, P. K., Webb, S. P., and Hammes-Schiffer, S. (2000). Computational studies of the mechanism for proton and hydride transfer in liver alcohol dehydrogenase. *Am. Chem. Soc.* 122 (19), 4803–4812. doi:10.1021/ja994456w

Aleku, G. A., France, S. P., Man, H., Mangas-Sanchez, J., Montgomery, S. L., Sharma, M., et al. (2017). A reductive aminase from *Aspergillus oryzae*. *Nat. Chem.* 9, 961–969. doi:10.1038/nchem.2782

An, J., Nie, Y., and Xu, Y. (2019). Structural insights into alcohol dehydrogenases catalyzing asymmetric reductions. *Crit. Rev. Biotechnol.* 39 (3), 366–379. doi:10.1080/07388551.2019.1566205

Bennett, M., Ducrot, L., Vergne-Vaxelaire, C., and Grogan, G. (2022). Structure and mutation of the native amine dehydrogenase MATOUAmDH2. *ChemBioChem* 23 (10), e202200136. doi:10.1002/cbic.202200136

Cai, R.-F., Liu, L., Chen, F.-F., Li, A., Xu, J.-H., and Zheng, G.-W. (2020). Reductive amination of biobased levulinic acid to unnatural chiral γ-amino acid using an engineered amine dehydrogenase. *ACS Sustain. Chem. Eng.* 8 (46), 17054–17061. doi:10.1021/acssuschemeng.0c04647

Caparco, A. A., Pelletier, E., Petit, J. L., Jouenne, A., Bommarius, B. R., de Berardinis, V., et al. (2020). Metagenomic mining for amine dehydrogenase discovery. *Adv. Synth. Catal.* 362 (12), 2427–2436. doi:10.1002/adsc.202000094

Chen, F., Zheng, G.-W., Liu, L., Li, H., Chen, Q., li, f., et al. (2018). Reshaping the active pocket of amine dehydrogenases for asymmetric synthesis of bulky aliphatic amines. *ACS Catal.* 8 (3), 2622–2628. doi:10.1021/acscatal.7b04135

Chen, F., Cosgrove, S. C., Birmingham, W. R., Mangas-Sanchez, J., Citoler, J., Thompson, M., et al. (2019). Enantioselective synthesis of chiral vicinal amino alcohols using amine dehydrogenases. *ACS Catal.* 9, 11813–11818. doi:10.1021/acscatal.9b03889

de Gonzalo, G., and Paul, C. E. (2021). Recent trends in synthetic enzymatic cascades promoted by alcohol dehydrogenases. *Curr. Opin. Green Sustain. Chem.* 32, 100548. doi:10.1016/j.cogsc.2021.100548

Ducrot, L., Bennett, M., Grogan, G., and Vergne-Vaxelaire, C. (2020). NAD(P)H-Dependent enzymes for reductive amination: Active site description and carbonyl-containing compound spectrum. *Adv. Synth. Catal.* 363 (2), 328–351. doi:10.1002/adsc.202000870

Ducrot, L., Bennett, M., Caparco, A. A., Champion, J. A., Bommarius Andreas, S., Zaparucha, A., et al. (2021). Biocatalytic reductive amination by native Amine Dehydrogenases to access short chiral alkyl amines and amino alcohols. *Front. Catal.* 1, 781284. doi:10.3389/fctls.2021.781284

Ducrot, L., Bennett, M., André-Leroux, G., Elisée, E., Marynberg, S., Fossey-Jouenne, A., et al. (2022). Expanding the substrate scope of native amine dehydrogenases through *in silico* structural exploration and targeted protein engineering. *ChemCatChem* 14, e202200880. doi:10.1002/cctc.202200880

Franklin, R. D., Mount, C. J., Bommarius, B. R., and Bommarius, A. S. (2020). Separate sets of mutations enhance activity and substrate scope of amine dehydrogenase. *ChemCatChem* 12, 2436–2439. doi:10.1002/cctc.201902364

González-Martínez, D., Cuetos, A., Sharma, M., García-Ramos, M., Lavandera, I., Gotor-Fernández, V., et al. (2020). Asymmetric synthesis of primary and secondary β-Fluoro-arylamines using reductive aminases from fungi. *ChemCatChem* 12 (9), 2421–2425. doi:10.1002/cctc.201901999

Hollmann, F., Opperman, D. J., and Paul, C. E. (2020). Biocatalytic reduction reactions from a chemist's perspective. *Angew. Chem. Int. Ed.* 60 (11), 5644–5665. doi:10.1002/anie.202001876

Jongkind, E. P. J., Fossey-Jouenne, A., Mayol, O., Zaparucha, A., Vergne-Vaxelaire, C., and Paul, C. E. (2022). Synthesis of chiral amines via a Bi-enzymatic cascade using an ene-reductase and amine dehydrogenase. *ChemCatChem* 14 (2), e202101576. doi:10.1002/cctc.202101576

Josef, B. K. W., and Winter, J. (1991). Purification and properties of F420 and NADP+-dependent alcohol dehydrogenases of *Methanogenium liminatans* and *Methanobacterium palustre*, specific for secondary alcohols. *Eur. J. Biochem.* 200, 43–51. doi:10.1111/j.1432-1033.1991.tb21046.x

Knaus, T., Bohmer, W., and Mutti, F. G. (2017). Amine dehydrogenases: efficient biocatalysts for the reductive amination of carbonyl compounds. *Green Chem.* 19 (2), 453–463. doi:10.1039/c6gc01987k

Krieger, E., Joo, K., Lee, J., Lee, J., Raman, S., Thompson, J., et al. (2009). Improving physical realism, stereochemistry, and side-chain accuracy in homology modeling: Four approaches that performed well in CASP8. *Proteins Struct. Funct. Bioinforma.* 77 (S9), 114–122. doi:10.1002/prot.22570

Kulig, J., Frese, A., Kroutil, W., Pohl, M., and Rother, D. (2013). Biochemical characterization of an alcohol dehydrogenase from *Ralstonia sp. Biotechnol. Bioeng.* 110 (7), 1838–1848. doi:10.1002/bit.24857

Lenz, M., Meisner, J., Quertinmont, L., Lutz, S., Kästner, J., and Nestl, B. M. (2017). Asymmetric ketone reduction by imine reductases. *ChemBioChem* 18 (3), 253–256. doi:10.1002/cbic.201600647

Lenz, M., Fademrecht, S., Sharma, M., Pleiss, J., Grogan, G., and Nestl, B. M. (2018). New imine-reducing enzymes from β-hydroxyacid dehydrogenases by single amino acid substitutions. *Protein Eng. Des. Sel.* 31 (4), 109–120. doi:10.1093/protein/gzy006

Liu, L., Wang, D.-H., Chen, F.-F., Zhang, Z.-J., Chen, Q., Xu, J.-H., et al. (2020). Development of an engineered thermostable amine dehydrogenase for the synthesis of structurally diverse chiral amines. *Catal. Sci. Technol.* 10, 2353–2358. doi:10.1039/d0cy00071j

Lu, J., Wang, Z., Jiang, Y., Sun, Z., and Luo, W. (2022). Modification of the substrate specificity of leucine dehydrogenase by site-directed mutagenesis based on biocomputing strategies. *Syst. Microbiol. Biomanuf.* doi:10.1007/s43393-022-00116-5

Ma, E. J., Siirola, E., Moore, C., Kummer, A., Stoeckli, M., Faller, M., et al. (2021). Machine-directed evolution of an imine reductase for activity and stereoselectivity. *ACS Catal.* 11 (20), 12433–12445. doi:10.1021/acscatal.1c02786

Marshall, J. R., Yao, P., Montgomery, S. L., Finnigan, J. D., Thorpe, T. W., Palmer, R. B., et al. (2020). Screening and characterization of a diverse panel of metagenomic imine reductases for biocatalytic reductive amination. *Nat. Chem.* 13, 140–148. doi:10.1038/s41557-020-00606-w

Mayol, O., David, S., Darii, E., Debard, A., Mariage, A., Pellouin, V., et al. (2016). Asymmetric reductive amination by a wild-type amine dehydrogenase from the thermophilic bacteria *Petrotoga mobilis*. *Catal. Sci. Technol.* 6 (20), 7421–7428. doi:10.1039/c6cy01625a

Mayol, O., Bastard, K., Beloti, L., Frese, A., Turkenburg, J. P., Petit, J.-L., et al. (2019). A family of native amine dehydrogenases for the asymmetric reductive amination of ketones. *Nat. Catal.* 2, 324–333. doi:10.1038/s41929-019-0249-z

Montgomery, S. L., Pushpanath, A., Heath, R. S., Marshall, J. R., Klemstein, U., Galman, J. L., et al. (2020). Characterization of imine reductases in reductive amination for the exploration of structure-activity relationships. *Sci. Adv.* 6 (21), eaay9320. doi:10.1126/sciadv.aay9320

Morris, G. M., Huey, R., Lindstrom, W., Sanner, M. F., Belew, R. K., Goodsell, D. S., et al. (2009). *J. Comput. Chem* 30, 2785–2791.

Prather, K. L. J. (2020). Accelerating and expanding nature to address its greatest challenges. *Nat. Catal.* 3 (3), 181–183. doi:10.1038/s41929-020-0422-4

Roiban, G.-D., Kern, M., Liu, Z., Hyslop, J., Tey, P. L., Levine, M. S., et al. (2017). Efficient biocatalytic reductive aminations by extending the imine reductase toolbox. *ChemCatChem* 9, 4475–4479. doi:10.1002/cctc.201701379

Roth, S., Präg, A., Wechsler, C., Marolt, M., Ferlaino, S., Lüdeke, S., et al. (2017). Extended catalytic scope of a well-known enzyme: Asymmetric reduction of iminium substrates by glucose dehydrogenase. *ChemBioChem* 18 (17), 1703–1706. doi:10.1002/cbic.201700261

Roth, S., Stockinger, P., Steff, J., Steimle, S., Sautner, V., Tittmann, K., et al. (2020). Crossing the border: From keto-to imine reduction in short-chain dehydrogenases/reductases. *ChemBioChem* 21 (18), 2615–2619. doi:10.1002/cbic.202000233

Sharma, M., Mangas-Sanchez, J., France, S. P., Aleku, G. A., Montgomery, S. L., Ramsden, J. I., et al. (2018). A mechanism for reductive amination catalyzed by fungal reductive aminases. *ACS Catal.* 8 (12), 11534–11541. doi:10.1021/acscatal.8b03491

Simić, S., Zukić, E., Schmermund, L., Faber, K., Winkler, C. K., and Kroutil, W. (2022). Shortening synthetic routes to small molecule active pharmaceutical ingredients employing biocatalytic methods. *Chem. Rev.* 122 (1), 1052–1126. doi:10.1021/acs.chemrev.1c00574

Tseliou, V., Knaus, T., Masman, M. F., Corrado, M. L., and Mutti, F. G. (2019). Generation of amine dehydrogenases with increased catalytic performance and substrate scope from ε-deaminating L-Lysine dehydrogenase. *Nat. Commun* 10 (1), 3717. doi:10.1038/s41467-019-11509-x

Tseliou, V., Schilder, D., Masman, M. F., Knaus, T., and Mutti, F. (2020). Generation of oxidoreductases with dual alcohol dehydrogenase and amine dehydrogenase activity. *Chem. Eur. J.* 27 (10), 3315–3325. doi:10.1002/chem.202003140

Wetzl, D., Gand, M., Ross, A., Müller, H., Matzel, P., Hanlon, S. P., et al. (2016). Asymmetric reductive amination of ketones catalyzed by imine reductases. *ChemCatChem* 8 (12), 2023–2026. doi:10.1002/cctc.201600384

Wu, S., Snajdrova, R., Moore, J. C., Baldenius, K., and Bornscheuer, U. T. (2020). Biocatalysis: Enzymatic synthesis for industrial applications. *Angew. Chem. Int. Ed.* 60 (1), 88–119. doi:10.1002/anie.202006648

Yang, Z. Y., Hao, Y. C., Hu, S. Q., Zong, M. H., Chen, Q., and Li, N. (2021). Direct reductive amination of biobased furans to N-substituted furfurylamines by engineered reductive aminase. *Adv. Synth. Catal.* 363 (4), 1033–1037. doi:10.1002/adsc.202001495

Ye, L. J., Toh, H. H., Yang, Y., Adams, J. P., Snajdrova, R., and Li, Z. (2015). Engineering of amine dehydrogenase for asymmetric reductive amination of ketone by evolving *rhodococcus* phenylalanine dehydrogenase. *ACS Catal.* 5 (2), 1119–1122. doi:10.1021/cs501906r

Zhang, J., Liao, D., Chen, R., Zhu, F., Ma, Y., Gao, L., et al. (2022). Tuning an imine reductase for the asymmetric synthesis of azacycloalkylamines by concise structure-guided engineering. *Ang. Chem. Int. Ed.* 61 (24), e202201908. doi:10.1002/anie.202201908